



**HAL**  
open science

## Synthesis and magnetic manipulation of hybrid nanobeads based on Fe<sub>3</sub>O<sub>4</sub> nanoclusters and hyaluronic acid grafted with an ethylene glycol-based copolymer

Marlène Rippe, Maxime Michelas, Jean-Luc Putaux, Mario Fratzl, Gabriel Gomez Eslava, Nora Dempsey, Rachel Auzély-Velty, Anna Szarpak

### ► To cite this version:

Marlène Rippe, Maxime Michelas, Jean-Luc Putaux, Mario Fratzl, Gabriel Gomez Eslava, et al.. Synthesis and magnetic manipulation of hybrid nanobeads based on Fe<sub>3</sub>O<sub>4</sub> nanoclusters and hyaluronic acid grafted with an ethylene glycol-based copolymer. *Applied Surface Science*, 2020, 510, pp.145354. 10.1016/j.apsusc.2020.145354 . hal-02897086

**HAL Id: hal-02897086**

**<https://hal.science/hal-02897086v1>**

Submitted on 18 Nov 2020

**HAL** is a multi-disciplinary open access archive for the deposit and dissemination of scientific research documents, whether they are published or not. The documents may come from teaching and research institutions in France or abroad, or from public or private research centers.

L'archive ouverte pluridisciplinaire **HAL**, est destinée au dépôt et à la diffusion de documents scientifiques de niveau recherche, publiés ou non, émanant des établissements d'enseignement et de recherche français ou étrangers, des laboratoires publics ou privés.

**Synthesis and magnetic manipulation of hybrid nanobeads based  
on Fe<sub>3</sub>O<sub>4</sub> nanoclusters and hyaluronic acid grafted with an  
ethylene glycol-based copolymer**

Marlène Rippe<sup>1</sup>, Maxime Michelas<sup>1</sup>, Jean-Luc Putaux<sup>1</sup>, Mario Fratzl<sup>2,3</sup>, Gabriel Gomez  
Eslava<sup>2</sup>, Nora M. Dempsey<sup>2</sup>, Rachel Auzély-Velty<sup>1</sup>, Anna Szarpak<sup>1,\*</sup>

<sup>1</sup>*Univ. Grenoble Alpes, CNRS, CERMAV, 38000 Grenoble, France*

<sup>2</sup>*Univ. Grenoble Alpes, CNRS, Grenoble INP, Institut Néel, 38000 Grenoble, France*

<sup>3</sup>*Univ. Grenoble Alpes, CNRS, Grenoble INP, G2Elab, 38000 Grenoble, France*

\* Corresponding author: email: [anna.szarpak@cermav.cnrs.fr](mailto:anna.szarpak@cermav.cnrs.fr)

## **Abstract**

Magnetic biopolymer hybrid nanoparticles have gained a lot of attention in the field of biomedical applications. Here we present the synthesis of hyaluronic acid (HA)-coated magnetic clusters of superparamagnetic nanoparticles. Firstly, the superparamagnetic magnetite nanoparticles coated with oleic acid were synthesized and characterized in terms of size, composition and magnetic properties. Secondly, magnetic nanoclusters were prepared and wrapped with HA grafted with an ethylene glycol-based copolymer. The resulting nanostructures and nanobeads were characterized using electron microscopy, dynamic light scattering, thermogravimetric analysis and magnetic measurements. The clustering of magnetite nanoparticles facilitates magnetic purification, separation, rapid attraction and controlled positioning by high field gradient micro-magnet arrays. In addition, clusters could be formed in the presence of a fluorescent drug model, which demonstrates the possibility of dual functionalization of our hybrid nanosystems: magnetic responsiveness and drug encapsulation.

## **Keywords**

Hyaluronic acid, magnetic nanoparticles, nanoclusters, micromagnet arrays, magnetic manipulation

## 1. Introduction

A lot of effort has been devoted to the design of multifunctional nanosystems combining different properties. Among these, the magnetic properties offered by iron oxide nanoparticles are particularly interesting and studied for biomedical applications. Magnetic nanoparticles (MNPs) may guide drugs to a site of interest in the body with the aid of a magnetic field, they can be used as contrast agents for magnetic resonance imaging (MRI) or they can be heated upon application of an alternating magnetic field to destroy cancer cells in hyperthermia treatment. They can also be used for separation of proteins, cells and bacteria, and in magnetic biosensors.<sup>1</sup>

Among a number of multifunctional magnetic nano- and microstructures, like magnetoliposomes,<sup>2</sup> magnetic micelles,<sup>3</sup> polymerosomes,<sup>4</sup> nanogels<sup>5</sup> and magnetic capsules,<sup>6,7</sup> polymeric systems are gaining a lot of interest as they provide numerous advantages. The coating of MNPs by a polymer layer leads to the development of hybrid systems where the polymer not only offers protection against uncontrolled aggregation of uncoated MNPs, thereby ensuring stability in a biofluid, but it also allows entrapment of therapeutic agents. Individual small (< 20 nm) superparamagnetic iron oxide nanoparticles (SPIONs) are not significantly responsive to a magnetic field. However, when concentrated in a polymer matrix, the increased magnetic moment of the overall object leads to an increase in responsiveness to a magnetic field, elevated diagnostic signal and heating efficiency.

Different synthetic or natural polymers have been tested to prepare magnetic hybrid nanostructures either by coating of individual MNPs or by aggregation of MNPs in a polymer matrix.<sup>3,8-15</sup> For biomedical applications, biocompatible natural polysaccharides like chitosan, dextran, alginate, cellulose and hyaluronic acid are highly attractive. Hyaluronic acid (HA), a linear polysaccharide naturally present in vertebrate tissues and body fluids, is particularly interesting due to its non-toxicity, biodegradability and biocompatibility.<sup>16</sup> In drug delivery

systems, HA is also sometimes used as a targeting molecule because it is recognized by cancer cells overexpressing the CD44 receptor.<sup>17,18</sup> Native HA does not interact with individual iron oxide nanocrystals, but its modification with dopamine allows it to complex and coat SPIONs. This approach ensures colloidal stability, better uptake and improved magnetic relaxivity in MRI.<sup>19-21</sup> Manju et al. formed a layer-by-layer film of HA and poly(*N*-vinyl-2-pyrrolidone) (PVP) on individual MNPs previously modified with aminosilane to create positive charges for electrostatic complexation with the first HA layer.<sup>22</sup> El-Dakdouki et al. used covalent conjugation of low molecular weight ( $M_w$ ) HA to amine containing SPIONs for MRI and doxorubicin (DOX) delivery.<sup>23</sup> In another approach the hydrophilic iron oxide nanostructures were incorporated into HA-based nanospheres fabricated via the water-in-oil emulsion technique. Firstly, HA was grafted with furan and maleimide groups, separately, to be later cross-linked via Diels-Alder chemistry in aqueous droplets dispersed in a mineral oil. Then hydrophilic magnetic nanostructures were added to an aqueous phase together with HA derivatives to be concentrated in a HA matrix and to allow quick heat generation under magnetic field.<sup>24</sup> The purification process, including centrifugation, precipitation and filtration with a wide range of organic solvents, seems to be technically challenging.

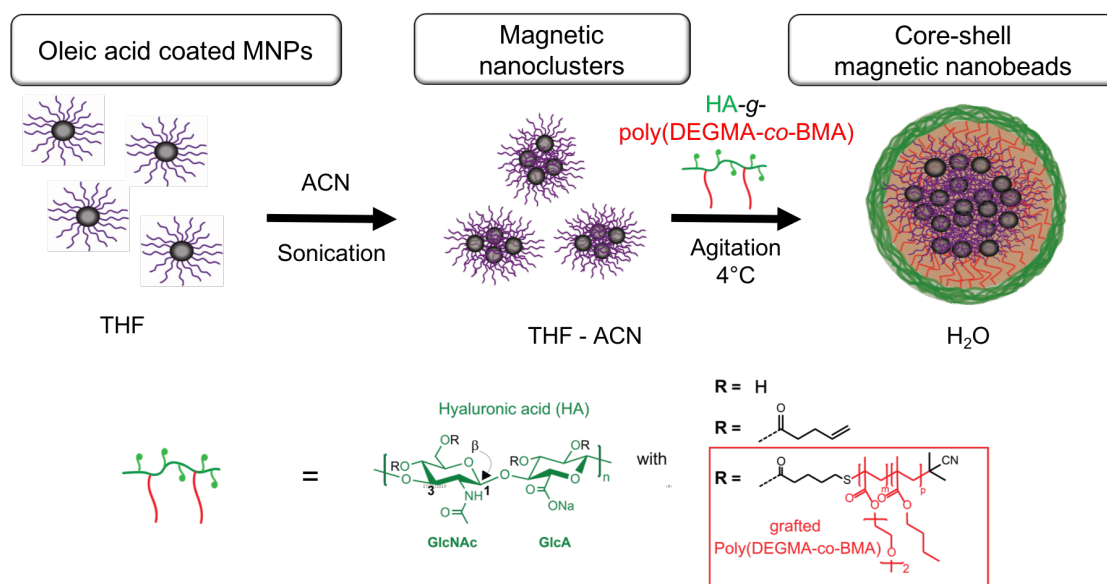
High-quality superparamagnetic iron oxide nanoparticles with uniform particle size distribution have been synthesized by thermal decomposition, a reaction which occurs in the presence of non-polar solvents and organic stabilizers (oleic acid/oleylamine).<sup>25</sup> However, such particles are insoluble in aqueous solutions and cannot be incorporated into a hydrophilic polymer matrix. Several approaches have been described to transfer hydrophobic nanoparticles from an organic to an aqueous solution. In the emulsion technique (oil-in-water), hydrophobic MNPs are enclosed in nanodroplets of organic solvent dispersed in an aqueous phase containing an amphiphilic polymer.<sup>26-28</sup> This technique has already been

applied to the incorporation of SPIONs in oleyl- or pyrenyl-modified hyaluronic acid to study selective recognition of CD44 receptor and tumor diagnosis using MRI.<sup>27,28</sup> However, the sonication used for homogenization of emulsions should be used with precaution especially for natural polymers such as HA, which is very sensitive and undergoes depolymerization under ultrasound treatment.<sup>29</sup> Another interesting method concerns the use of thermoresponsive polymers which self-assemble into micelles when heated and simultaneously enclose magnetic nanoparticles.<sup>3,30</sup> Pellegrino et al. reported the formation of hydrophobic magnetic nanoclusters in the presence of a synthetic amphiphilic polymer. Colloidal nanoclusters were formed via the solvent destabilization method which exploits a change of solvent polarity. In this case, the hydrophobic MNPs dissolved in tetrahydrofuran (THF) tended to self-assemble after the addition of acetonitrile (ACN) while the presence of poly(maleic anhydride-*alt*-1-octadecene), which undergoes partial hydrolysis, stabilized nanoclusters in aqueous conditions.<sup>15,31</sup> It should be noted that neither of the last two mentioned methods have ever been tested for the fabrication of magnetic-composites with HA.

In the past five years, our research group developed various HA derivatives modified with thermoresponsive ethylene glycol-based copolymers for the formation of well-defined nanogels via temperature-induced self-assembly.<sup>32-35</sup> These HA-copolymer conjugates are soluble in aqueous solutions below the cloud point temperature ( $T_{cp}$ ) of the grafted copolymer and form nanogels above this temperature. They showed great potential for the encapsulation of hydrophobic drugs in hydrophobic nanodomains made of the grafted copolymer chains, good stability in dilute conditions and prolonged blood circulation after hydrophobic core or hydrophilic shell cross-linking.

The aim of this study was to investigate the ability of HA modified with poly(di(ethylene glycol) methacrylate-*co*-butyl methacrylate) (HA-*g*-poly(DEGMA-*co*-BMA) to encapsulate

hydrophobic MNPs to obtain magnetic composites that can be efficiently manipulated with magnetic fields. We have tested the solvent destabilization technique for the formation of nanoclusters highly loaded with MNPs and coated with the HA-copolymer conjugate. We hypothesized that this HA derivative could act as an efficient stabilizing agent of magnetic nanoclusters via hydrophobic interactions. The strategy for the synthesis of the HA-based magnetic nanohybrids includes (i) synthesis of hydrophobic superparamagnetic NPs, (ii) formation of nanoclusters and (iii) assembly of HA-copolymer conjugate on the nanocluster, as presented in Scheme 1.



**Scheme 1.** Schematic representation of the formation of core-shell magnetic nanobeads.

To this end, the hydrophobic superparamagnetic NPs were synthesized and characterized in terms of size, composition and magnetic properties. The obtained superparamagnetic nanoparticles were employed for cluster formation using the solvent destabilization technique. Finally, the stabilization of clusters with HA-g-poly(DEGMA-co-BMA), allowing the formation of nanobeads, is described. The nanobeads were characterized by scanning and transmission electron microscopy (SEM and TEM), dynamic light scattering (DLS),

thermogravimetric analysis (TGA) and magnetometry. Finally, magnetic trapping and alignment of the nanobeads was demonstrated using an array of micro-magnets.

## **2. Materials and methods**

### *2.1. Materials*

Hyaluronic acid HA20 ( $M_w = 20 \text{ kg mol}^{-1}$ ) was purchased from Lifecore (USA). Phosphate buffer saline (PBS, pH 7.4), 1,4-dithiothreitol (DTT), tris-(2-carboxyethyl) phosphine hydrochloride (TCEP) were purchased from Sigma (France). 2-Hydroxy-1-[4-(2-hydroxyethoxy)phenyl]-2-methyl-1-propanone (Irgacure 2959) was kindly provided by Ciba Specialty Chemicals (Basel, Switzerland). The dye di-strylbenzene derivative (DSB) was kindly provided by Olivier Stephan (Université Grenoble Alpes, Grenoble, France). The positively charged resin, diethylaminoethyl cellulose (DEAE Sepharose CL-6B) was purchased from GE Healthcare Life Science. The Spectra/Por 1 ( $MWCO 6-8000 \text{ g mol}^{-1}$ ) membrane used for dialysis was obtained from Fisher Scientific (Rancho Domingez, CA). The water used in all experiments was purified by an Elga Purelab purification system, with a resistivity of  $18.2 \text{ M}\Omega\cdot\text{cm}$ . The pentenoate-modified hyaluronic acid (HAp) with a degree of substitution (DS or average number of substituents per repeating unit) of 0.4 and copolymer poly(DEGMA-co-BMA) were synthesized as previously described<sup>35</sup>. Oleic acid (90%) was from Fischer Scientific. Iron(III) acetylacetonate, 1,2-hexadecanediol (97%), oleylamine (>70%), were purchased from Aldrich Chemical Co. A bulk NdFeB cylindrical magnet of diameter 8 mm and height 20 mm with magnetic remanence 1.2 T was purchased from Chen Yang Technologies GhhH&Co.KG.

### *2.2. Synthesis of HA-g-poly(DEGMA-co-BMA)*

HA-g-poly(DEGMA-co-BMA) was synthesized according to the procedure described before.<sup>35</sup> In short, the poly(DEGMA-co-BMA) copolymer was subjected firstly to aminolysis using *n*-butylamine, to convert the reversible addition–fragmentation chain transfer (RAFT) end-group to a thiol. Next, the thiol-end-functionalized copolymer was solubilized in pure water and TCEP was added. After 30 min of stirring at 4 °C under nitrogen atmosphere, the copolymer solution was added to a solution of HA-pentenoate in pure water, followed by addition of Irgacure 2959. The reaction mixture was cooled in an ice bath and exposed to UV light ( $\lambda = 365$  nm) with an intensity of 20 mW cm<sup>-2</sup> for 5 min under stirring and nitrogen atmosphere. The resulting HA-g-poly(DEGMA-co-BMA) was purified via a batch ion exchange process using DEAE Sepharose CL-6B as a weak-anion exchanger. Finally, the solution was dialyzed against deionized water (membrane with cut-off 6-8 Da MW, 72 h). The product was recovered as a white powder by freeze-drying. The DS was indirectly determined by reaction of D-glucuronic acid units of HA with carbazole.<sup>35,36</sup>

### 2.3. Synthesis of iron oxide nanoparticles

The monodisperse magnetic nanoparticles (MNPs) were prepared according to a slightly modified procedure.<sup>37–39</sup> In short, iron III acetylacetonate (Fe(acac)<sub>3</sub>), 1,2-tetradecanediol, oleic acid, oleylamine and benzyl ether were mixed and degassed at room temperature for 30 min under a constant flow of N<sub>2</sub> and vigorous stirring. Next, the solution was heated up at 3 °C min<sup>-1</sup> and kept at 200 °C for 2 h followed by a second heating at 4.5 °C min<sup>-1</sup> up to 300 °C. After 1 h, the resultant black-colored mixture was cooled to RT, nanoparticles precipitated and washed using EtOH.

### 2.4. Synthesis of core/shell nanobeads

Oleic acid coated iron oxide magnetic nanoparticles (MNPs) were dissolved in 200  $\mu\text{L}$  of tetrahydrofuran ( $1 \text{ mg mL}^{-1}$ ) under sonication. 200 $\mu\text{L}$  of destabilizing solvent (ACN) was added to the suspension of MNPs at a rate of  $250 \text{ }\mu\text{L min}^{-1}$  and sonicated for 20 min at  $70 \text{ }^\circ\text{C}$  to evaporate THF. Then the nanocluster suspension was placed in an ice bath at  $4 \text{ }^\circ\text{C}$ . One mL (0.5 g) of cold aqueous solution of HA-g-poly(DEGMA-co-BMA) with DS of 0.02 was slowly added to the nanoclusters and agitated for 15 min at RT. The vial containing the magnetic nanobeads was brought into contact with the bulk permanent magnet for 4 h, the supernatant was removed and fresh milli-Q water added (repeated twice). Separation of agglomerates was performed by contact between the vial and the bulk magnet for 15 min.

### *2.5. Cross-linking of core-shell nanobeads*

25  $\mu\text{L}$  of DTT in water ( $2.5 \text{ g L}^{-1}$ ) was added to the sample of nanobeads obtained after addition of 1 mL ( $0.5 \text{ g L}^{-1}$ ) HA-g-poly(DEGMA-co-BMA) to the magnetic nanoclusters. Finally, an aqueous solution of Irgacure 2959 ( $10 \text{ mg mL}^{-1}$ ) was added to the suspensions to obtain a final photoinitiator concentration of 10% (w/v). The mixture was exposed to UV light ( $\lambda = 365 \text{ nm}$ ) with an intensity of  $20 \text{ mW cm}^{-2}$  for 15 min under stirring and nitrogen atmosphere. The sample was further purified using the bulk magnet.

### *2.6. In situ encapsulation of MNPs*

The MNPs suspended in chloroform ( $16 \text{ mg mL}^{-1}$ ) were added drop-by-drop ( $30 \text{ }\mu\text{L}$ , 0.5 mg) into a solution of HA-g-poly(DEGMA-co-BMA) in 1 mL of PBS at  $4 \text{ }^\circ\text{C}$  under vortex followed by a temperature increase up to  $40 \text{ }^\circ\text{C}$ . After 30 min of stirring, the cross-linking procedure similar to that for core-shell nanobeads was applied at  $40 \text{ }^\circ\text{C}$ . The magnetic nanogel suspension was transferred into a dialysis bag (MWCO = 6–8000  $\text{g mol}^{-1}$ ) and

dialyzed against deionized water for 72 h. The nanogels were recovered by freeze-drying and analyzed by TGA.

### *2.7. Loading of DSB into magnetic nanobeads*

50  $\mu\text{L}$  of DSB dissolved in THF ( $0.5 \text{ mg mL}^{-1}$ ) were added to a 200  $\mu\text{L}$  of MNPs in THF ( $1 \text{ mg mL}^{-1}$ ). The mixture was sonicated for 20 min followed by addition of 250  $\mu\text{L}$  of ACN (THF/ACN, 1/1). After 20 min of further sonication, at 70  $^{\circ}\text{C}$  to evaporate THF, the sample was cooled in ice before adding 1 mL ( $0.5 \text{ mg}$ ) of HA-*g*-poly(DEGMA-*co*-BMA) in  $\text{H}_2\text{O}$ . After 30 min of agitation, the sample was placed close to the bulk magnet for 4h to remove supernatant and to collect the nanobeads loaded with magnetic nanoparticles and DSB. The supernatant containing a mixture of solvents and unloaded DSB was removed and replaced with 1 mL of water (repeated twice). Finally, the fluorescent nanobeads were re-dispersed in water or PBS.

### *2.8. Micro-patterned hard magnetic films*

5  $\mu\text{m}$ -thick hard-magnetic neodymium iron boron (NdFeB) films deposited on Si wafers were firstly magnetized out of plane in 8 T and then irradiated with a KrF (248 nm) pulsed excimer laser during 20 ns.<sup>40</sup> During irradiation, a chessboard mask consisting of a pattern with individual features of size  $100 \times 100 \mu\text{m}^2$  or a stripe mask consisting of patterns with individual feature sizes of  $3 \text{ mm} \times 100 \mu\text{m}$  was placed in front of the film and a magnetic field was applied in the direction opposite to the initial magnetization direction. As a result, the exposed magnetic regions were heated by the laser and the magnetization direction was reversed. The resultant structures consist of either a chessboard type or a stripe type array of oppositely magnetized micro-magnets. Magnetic field gradients as high as  $10^6 \text{ T m}^{-1}$  are produced by these thermomagnetically patterned films.<sup>41</sup> A 20  $\mu\text{L}$  drop of the nanobead

solution was dropped onto a glass coverslip and flattened with the micro-patterned magnetic surface. The precise patterns formed by the distribution of the nanobeads due to their attraction to the micro-magnet array were imaged using an inverted fluorescence optical microscopy (Olympus CKX41).

## *2.9. Characterization methods*

### Scanning electron microscopy (SEM)

Drops of nanobead suspensions in ultrapure water were deposited onto carbon adhesive tabs and allowed to dry in air overnight at RT. The samples were then coated by approximately 2 nm of sputtered Au-Pd and observed with a ZEISS Ultra 55 microscope equipped with a field-emission gun (FEG). Images were acquired at a low voltage of 3 kV using an in-lens secondary electron imaging detector.

### Transmission electron microscopy (TEM) and cryo-TEM

200-mesh TEM grids coated with a thin film of amorphous carbon were submitted to a glow discharge treatment (Pelco easiGlow) to make the surface of the carbon film hydrophilic. Droplets (4  $\mu$ L) of dilute particle suspensions were deposited on the grid and, after a few minutes, the liquid in excess was blotted with filter paper. Prior to complete drying, droplets of Uranyless<sup>TM</sup> (neutral contrast agent, Delta Microscopies) were deposited. After a few minutes, the stain in excess was blotted out and the remaining liquid film allowed to dry. Images of the specimens were recorded with a TVIPS TemCam F216 digital camera, using a Philips CM200 'Cryo' (FEI) microscope operating at 200 kV. The particle size was measured from the TEM images using the ImageJ software. The statistical size distribution was evaluated from approximately 200 particles. For cryo-TEM imaging, thin liquid films of the suspensions were formed on NetMesh lacey carbon films (Pelco) and quench-frozen in

liquid ethane using a Leica EM-GP workstation. The specimens were mounted on a precooled Gatan 626 specimen holder, transferred to the Philips CM200 'Cryo' microscope and observed at low temperature (-176 °C).

#### Fourier transform infrared (FTIR) spectroscopy

FTIR measurements were made on a RX1 spectrometer (Perkin Elmer, UK) with horizontal ATR accessory. For each sample, 32 scans were recorded between 4000 and 400  $\text{cm}^{-1}$  with a resolution of 2  $\text{cm}^{-1}$  using the Spectrum Software V 5.0.0.

#### Dynamic light scattering (DLS)

Particle size measurements were carried out by dynamic light scattering (DLS) using a Malvern Instruments Zetasizer Nano series instrument. Measurements were conducted at 18 °C on 1 mL volume sample in PBS (pH 7.4).

#### Thermogravimetric analysis (TGA)

The amount of MNPs encapsulated inside HA-*g*-poly(DEGMA-*co*-BMA) structures was determined by thermogravimetric analysis using a TGA 92, Setaram Instruments. The samples were analyzed under  $\text{N}_2$  (1 bar) and at a heating rate of 5 °C  $\text{min}^{-1}$  from 25 to 700 °C.

#### SQUID-VSM analysis

The magnetic properties of the MNP and the nanobeads were evaluated using a superconducting quantum interference device (SQUID) - VSM (Vibrating Sample Magnetometer) from Quantum Design. The MNPs were dispersed in polydimethylsiloxane (PDMS), while the magnetic nanobeads were freeze-dried. Magnetization loops were

measured at 5 and/or 300 K and the results were corrected by subtracting the diamagnetic contribution of the sample holder. Temperature dependent zero-field cooled and field cooled magnetization measurements were performed by cooling the sample to 5 K under a zero or a 100 Oe magnetic field, respectively. Magnetization was then measured while the samples were heated to 300 K under a 100 Oe field.

### Fluorescence imaging

The trapping of magnetic nanobeads was observed using an Olympus inverted research microscope iX71 equipped with a mercury burner U-RFL-T as light source and a digital camera Olympus DP70 for image acquisition. Blue excitation light ( $450 \leq \lambda \leq 480$  nm) and green emission light ( $\lambda \leq 515$  nm) was filtered using a U-MWB Olympus filter cube. Green excitation ( $510 \leq \lambda \leq 550$  nm) and red emission light ( $\lambda \geq 590$  nm) were filtered using a U-MWG Olympus filter cube.

## 3. Results and Discussion

### 3.1. Synthesis and characterization of iron oxide magnetic nanoparticles

Monodisperse magnetic nanoparticles were synthesized using thermal decomposition, as previously reported.<sup>37–39</sup> The size of individual MNPs was investigated using TEM analysis (Fig. 1A) showing nanocrystals with a size of  $7.8 \pm 0.8$  nm. The selected area powder electron diffraction pattern recorded from a group of particles indicated that the MNPs were crystalline, corresponding to Fe<sub>3</sub>O<sub>4</sub> magnetite (Supporting Information Fig. S1).<sup>42</sup>

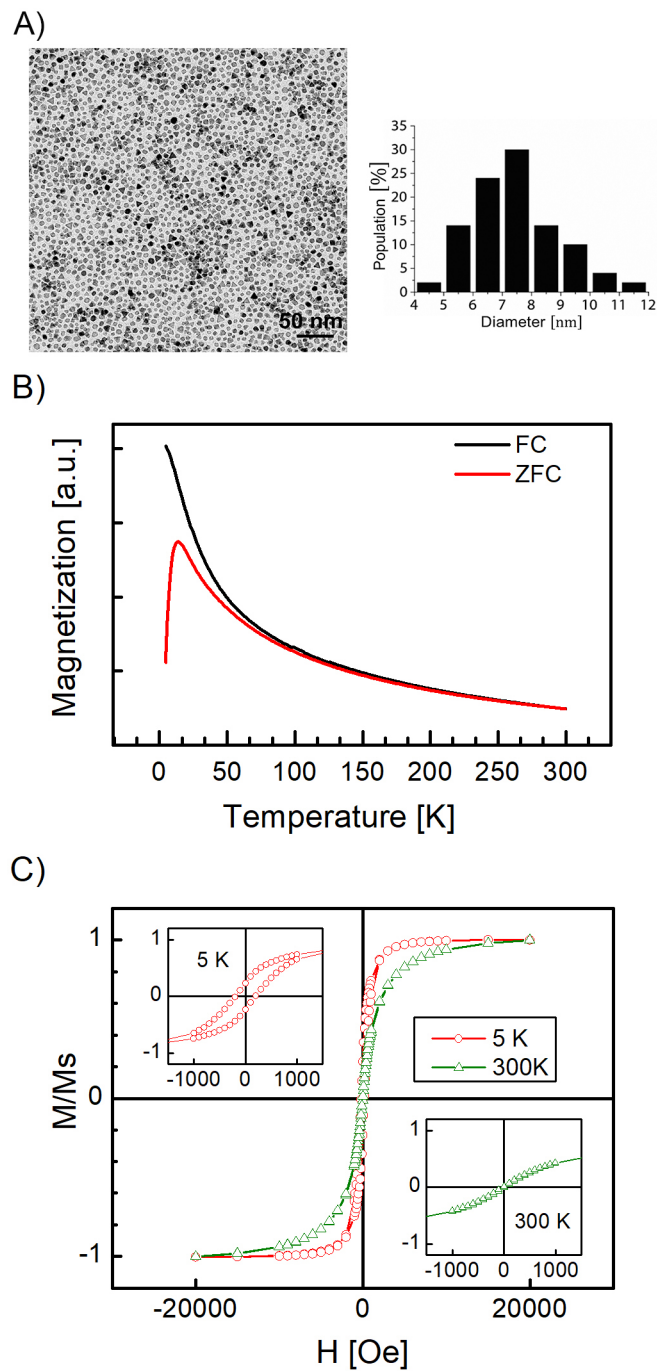


**Figure 1.** A) TEM image of synthesized MNPs and size distribution histogram determined from the TEM image; B) Temperature dependence of magnetization of MNPs under ZFC-FC conditions measured at 100 Oe; C) Normalized magnetization ( $M/M_s$ ) vs applied magnetic field ( $H$ ) loops measured at 5 and 300 K. Insets: The expanded views of hysteresis loops at 5 and 300 K.

Thermogravimetric analysis (TGA) and FT-IR spectra were recorded to confirm the presence of hydrophobic ligands on the surface of the MNPs. TGA showed a significant weight loss between 200 – 450 °C due to the decomposition of organic coating ligands (oleic acid and oleylamine) present on the surface of inorganic NPs (Fig. S2A). FT-IR of MNPs in comparison with oleylamine and oleic acid spectra, respectively, are presented in Fig. S2B. Three distinct regions stand out with coated MNPs: alkyl chains (3000 - 2800  $\text{cm}^{-1}$ ),  $\text{COO}^-$  groups of oleic acid (1800 - 900  $\text{cm}^{-1}$ ) and Fe-O links of iron oxide (800 - 400  $\text{cm}^{-1}$ ). Compared to the spectra of oleic acid and oleylamine, two bands at 2922 and 2849  $\text{cm}^{-1}$ , characteristic for asymmetric and symmetric  $\text{CH}_2$  stretches, respectively, are present on MNPs spectra. The intense C=O stretch band of the carboxyl group of oleic acid at 1730  $\text{cm}^{-1}$  could also be observed on MNPs and two new bands at 1564 and 1400  $\text{cm}^{-1}$  appeared, which are characteristic of asymmetric and symmetric  $\text{COO}^-$  stretches, respectively, due to the bonding of carboxylic groups to the surface of iron oxide nanoparticles.<sup>40</sup> Due to the presence of hydrophobic chains, our NPs were highly colloidal stable in organic solvents such as hexane, toluene, tetrahydrofuran or chloroform, but unstable in water.

The magnetization measurements confirmed superparamagnetic behavior of the synthesized MNPs. The zero field-cooled (ZFC) curve exhibited a peak at 20 K, indicating a transition from a magnetically blocked state (at  $T < 20$  K) to a superparamagnetic state (Fig. 1B). Figure 1C shows VSM magnetization curves of MNPs measured at 5 and 300 K, with low-field zooms shown as insets. The 5 K hysteresis loop indicates ferromagnetic behavior with a coercivity of 200 Oe. In contrast, the  $M/M_s$  vs  $H$  curve of the MNPs at 300 K shows no hysteresis or remanence, thus confirming their superparamagnetic behavior at this temperature.

We also tested the magnetic attraction of individual MNPs (~8 nm) dispersed in THF. Overnight contact of the sample vial with the bulk NdFeB magnet was not sufficient to attract

all ultra-small MNPs (Fig. S2C). Such ultra-small MNPs exhibit low magnetic moment, reducing their responsiveness to the bulk magnet.

### 3.2. Characterization of HA-g-poly(DEGMA-co-BMA)

Hyaluronic acid ( $M_w = 20 \text{ kg mol}^{-1}$ ) was partially grafted with di(ethylene glycol) methacrylate-co-butylmethacrylate (poly(DEGMA-co-BMA)) as described previously.<sup>35</sup> The polysaccharide was first esterified with pentenoic anhydride to produce ene-functional chain that can react with poly(DEGMA-co-BMA) bearing the RAFT group converted to thiol before reaction under UV irradiation.

Before grafting, the composition of the copolymer was analyzed.  $^1\text{H}$  NMR and size exclusion chromatography (SEC) analysis of the poly(DEGMA-co-BMA) revealed a copolymer composition DEGMA/BMA of 95:5, a low dispersity ( $D = 1.12$ ), and a number average molar mass  $M_n$  of  $\sim 16 \text{ kg/mol}$  ( $M_{n,\text{NMR}} = 15500 \text{ g mol}^{-1}$ ,  $M_{n,\text{SEC}} = 15740 \text{ g mol}^{-1}$ , (Fig. S3).

Successful grafting of copolymer on HA was confirmed by  $^1\text{H}$  NMR analysis. The proton signals at 4.29, 3.89, 3.48 and in the region of 0.99-1.2 ppm belonging to copolymer (Fig. S4A) could be observed. The degree of substitution (DS; defined as the number of poly(DEGMA-co-BMA) chains per 100 disaccharides repeating units), determined by the carbazole assay,<sup>35,36</sup> was found to be  $0.02 \pm 0.01$ , corresponding to copolymer content in HA-conjugate of 43 % (in weight). The FT-IR of HA-conjugate in comparison with native HA, HA-pentanoate (HAp) and poly(DEGMA-co-BMA) spectra, respectively, are presented in Figure S4B. The HA-g-poly(DEGMA-co-BMA) shows characteristic signals of HA such as the bands at about  $1620 \text{ cm}^{-1}$  corresponding to the amide carbonyl,  $1410 \text{ cm}^{-1}$  attributed to the stretching of  $\text{COO}^-$  and at  $1042 \text{ cm}^{-1}$  attributed to the stretching of C-OH. The signal at  $1725$

cm<sup>-1</sup> related to the carbonyl stretching of the methacrylate comonomer increased after grafting on HAp chains.

### 3.3. Synthesis and characterization of HA-g-poly(DEGMA-co-BMA) magnetic nanobeads

The formation of magnetic nanoclusters followed by HA-g-poly(DEGMA-co-BMA) coating is presented in Scheme 1. Firstly, the hydrophobic MNPs were dissolved in THF (1 g L<sup>-1</sup>) followed by a slow addition of ACN (250  $\mu$ L min<sup>-1</sup>), under sonication. The MNPs are not stable in polar solvents, thus the presence of ACN induces the formation of hydrophobic nanoclusters. As reported previously, under such conditions, the MNPs tend to densely pack in the THF nanodroplets. However, clustering was performed in the presence of P18 (poly(maleic anhydride-*alt*-1-octadecene)) which allowed direct enwrapping of hydrophobic nanoparticles. After partial hydrolysis of P18, the nanoclusters were shown to be stable in aqueous solvent.<sup>31</sup> In our case, we performed clustering without the addition of a stabilizing agent. After 20 min of sonication of MNPs in THF/ACN (1/1 v/v) at 70 °C to evaporate THF, the nanocluster suspension was cooled and mixed with 1 mL of a cold solution of HA-g-poly(DEGMA-co-BMA) (0.5 g L<sup>-1</sup>, 4 °C) using an orbital shaker. Magnetic stirring was excluded due to the attraction of nanobeads by the magnetic bar. Note that sonication was used only for cluster formation, while the deposition of HA-copolymer conjugate on cluster surfaces was performed under gentle mixing to avoid possible HA depolymerization.

We have recently shown that thermoresponsive HA-g-poly(DEGMA-co-BMA) is able to self-associate and form nanogels by increasing the temperature above its T<sub>cp</sub>.<sup>35</sup> However, T<sub>cp</sub> can be changed by the addition of salts, surfactants or solvents to a thermoresponsive polymer/water system. In this particular case, HA-g-poly(DEGMA-co-BMA) is well dissolved in water at 4 °C, but once added to hydrophobic nanoclusters dispersed in THF/ACN, the final suspension became cloudy. Possibly, under these conditions, the

copolymer grafted on HA chains becomes hydrophobic, with a high affinity for the nanoclusters, and tends to adsorb on their surfaces with the hydrophilic HA oriented towards the surrounding water.

The formed beads were temporarily attracted by the bulk NdFeB magnet, allowing removal of the mixture of solvents in which they were suspended (Fig. 2). After removal of the supernatant, the magnetic nanobeads were re-dispersed perfectly in water and easily collected again using the bulk magnet. The zeta potential measurements ( $-29 \pm 5$  mV) confirmed the presence of a negative HA shell.

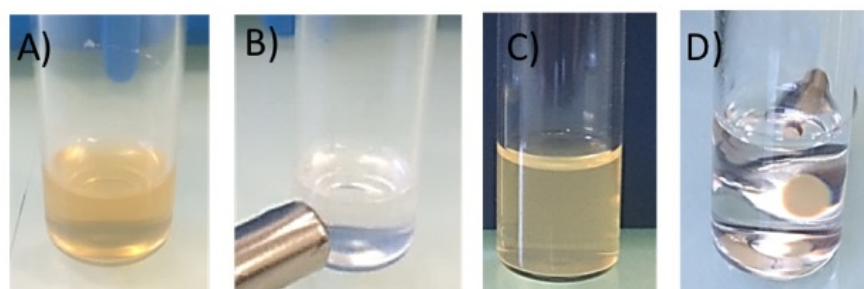


**Figure 2.** A) Nanobead suspensions: directly after HA-g-poly(DEGMA-co-BMA) assembly; B) after 4 h of separation from solvents with the bulk magnet; C) re-dispersed in water; D) re-attracted by the bulk magnet.

SEM images show nanosized objects with bright cores and surrounding shells (Figs. 3A). The bright contrast of the core is likely due to the presence of a constituent with a higher atomic number. The morphology is confirmed by TEM images that show spheroidal nanobeads with a diameter ranging from 100 to 250 nm and containing a dark MNP core (Fig. 3B). Higher magnification images show that the magnetic cluster is constituted of close-packed MNPs and encased in an outer polymer shell (Fig. 3C). A similar core-shell organization was observed by cryo-TEM of ice-embedded nanoparticles (Fig. 3D). Individual MNPs can be observed in the macromolecular shell, possibly corresponding to NPs that

detached from the core surface and diffused into the HA shell which contains hydrophobic domains of grafted copolymer.

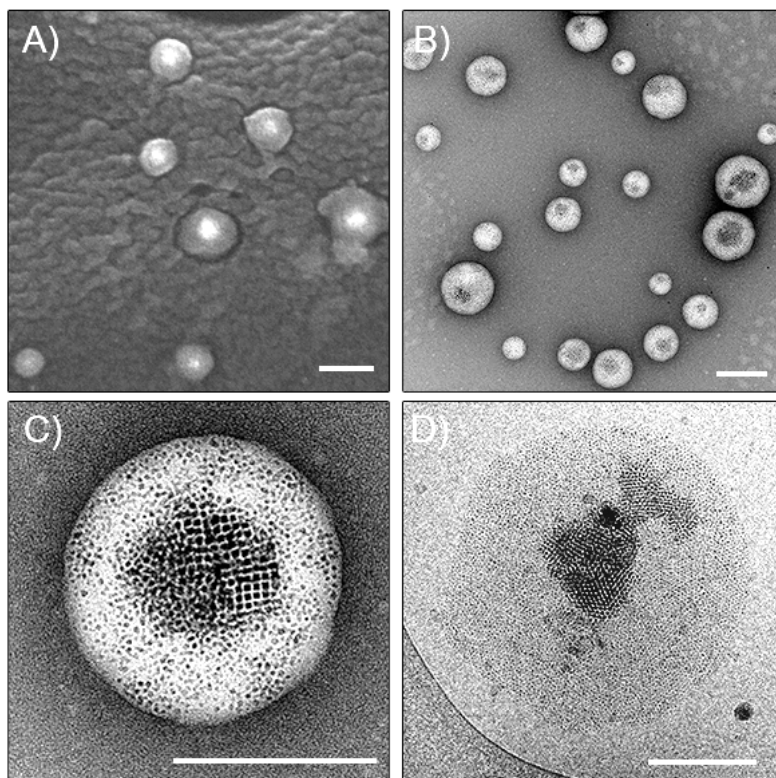


**Figure 3.** SEM (A), TEM with negative staining (B,C), and cryo-TEM (D) images of HA-g-poly(DEGMA-co-BMA)-coated magnetic nanoclusters. Scale bar: 200 nm.

In order to collect such small nanobeads from the suspension presented in Figure 2C, which contains also bigger nanostructures of a few hundred nanometers (agglomerates/interconnected clusters), magnetic separation was applied. When the bulk magnet was brought in contact with the vial, after just 15 min the biggest structures had been attracted to the magnet while the smaller ones (< 250 nm) remained in the supernatant. Figure S5 shows TEM and SEM images of nanobeads before separation (A,B) and nanobeads remaining in the supernatant after 15 min of contact with the magnet (C,D).

To confirm the role of HA-g-poly(DEGMA-co-BMA) in the formation of well-dispersed magnetic nanobeads, control experiments were performed. The formation of different

structures was observed when clusters were: i) without polysaccharide coating, ii) mixed with HA without grafted copolymer, and iii) mixed with pure poly(DEGMA-*co*-BMA). In all three cases, we observed the precipitation or uncontrolled dispersion of MNPs in the polymer matrix (Fig. S6). Thus, employing the HA grafted with the ethylene glycol-based copolymer was necessary to stabilize the magnetic nanoclusters. The HA protects the magnetic nanoclusters from uncontrolled aggregation, ensures stability and easy dispersion in aqueous conditions.

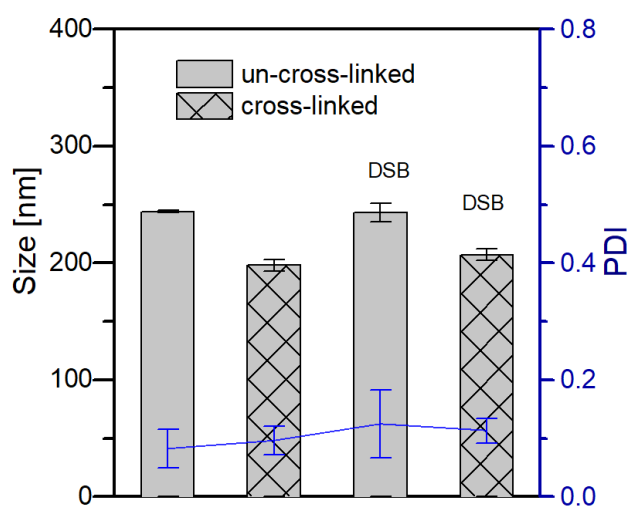


**Figure 4.** Hydrodynamic diameter and polydispersity index (PDI - blue) of un-crosslinked and crosslinked nanobeads, with and without DSB, in PBS (pH 7.4) at 18 °C measured by DLS.

The DLS analysis carried out in PBS buffer (pH 7.4) showed the hydrodynamic diameter of un-cross-linked nanobeads to be  $244 \pm 1$  nm (Fig. 4). Cross-linking of the shell, using bis-thiol agent 1,4-dithiothreitol (DTT), which forms thio-ether bonds with the remaining pentenoate groups of HA chains through radical thiol-ene chemistry,<sup>35</sup> resulted in a nanobead size of  $\sim 200$  nm. Although we could observe a slight effect of cross-linking on the size of the nanobeads (indicating a reinforcement of the HA shell structure), nanobeads without cross-linking were stable for a long time, showing a size of  $238 \pm 7$  nm (DLS measurements after 3

months). It can be assumed that strong hydrophobic interactions between the hydrophobic magnetic core and the copolymer present on HA chains make the structure intact.

For comparison, *in situ* encapsulation of MNPs during self-assembly of thermoresponsive HA-g-poly(DEGMA-co-BMA) was tested (Figs. S7 and S8). It has been shown earlier that this HA derivative modified with ethylene-based copolymers was able to form soft nanoparticles called "nanogels".<sup>35</sup> Here, the MNPs in chloroform were injected to a cold aqueous solution of HA-g-poly(DEGMA-co-BMA) followed by an increase of temperature up to 40 °C and cross-linking (self-associated nanogels were not stable without cross-linking). Although we observed the formation of polymeric nanostructures due to the self-association of thermoresponsive HA chains ( $T_{cp} = 20$  °C), the distribution of MNPs was non-homogenous (Fig. S8) and the content of inorganic particles was lower than in the case of core-shell nanobeads (Fig. 5). TGA measurements were performed on core-shell nanobeads and thermoresponsive nanogels with enclosed MNPs (Figure 5).

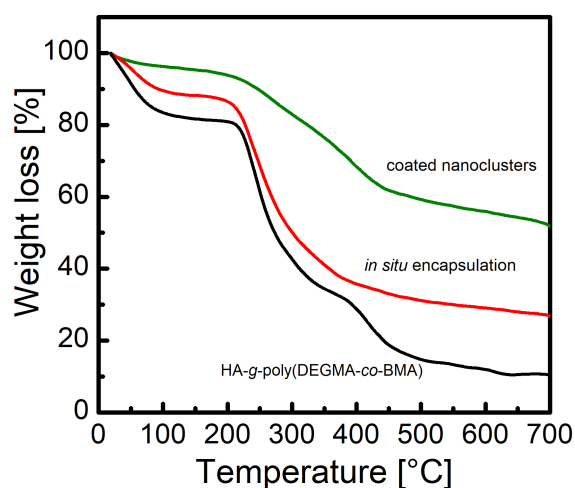


**Figure 5.** Thermogravimetric analysis (TGA) curves of pure HA-g-poly(DEGMA-co-BMA) (black), HA-g-poly(DEGMA-co-BMA) coated nanoclusters (green) and nanogels with *in situ* encapsulated MNPs (red), analyses were performed under N<sub>2</sub> atmosphere, all samples were freeze dried before analysis.

Firstly, to understand the decomposition of the polymer residue of hybrid nanostructures, pure HA-g-poly(DEGMA-co-BMA) polymer was analyzed. The curve of the HA derivative exhibits three zones of weight loss from 40 to 700 °C, reaching a total weight loss of 90 %. The first occurs in the 40-120 °C temperature range, corresponding to the evaporation of residually bound water. Two further zones of weight loss begin at around 220 and 400 °C, corresponding to the decomposition of HA and DEGMA-co-BMA copolymer grafted on HA chains, respectively. Heating to 700 °C resulted in a final weight of 10 % residual weight. Similar steps of decomposition were previously observed for membranes composed of HA and polyethylene oxide (PEO), with decomposition of PEO starting at 411 °C and final resistance of HA for complete decomposition.<sup>45</sup> Finally, TGA curves of magnetic nanohybrids were measured. The formulation, 0.4 and 1 mg of MNPs per mg of HA-g-poly(DEGMA-co-BMA) for core/shell and *in situ* encapsulation, respectively, was used. For both studied systems, decomposition of HA-g-(DEGMA-co-BMA) begins at 200 °C. At 450 °C the sample weight begins to stabilize. From the weight residues at 700 °C, the quantity of magnetic nanoparticles in these two different nanocomposites could be estimated. As the quantity of residual water in pure HA-copolymer, core-shell nanobeads and thermoresponsive nanogels is different, the percentage of magnetic nanoparticles in hybrid samples was estimated after normalization of sample weight at 200 °C (after evaporation of residually bound water) and subtraction of the residue of non-decomposed polysaccharide at 700 °C (Fig. S9).

Finally, we could estimate that the percentage of magnetic material, i.e. the MNP content of the core-shell nanobeads, was close to 44%. This is 2.5 times higher than in the case of *in situ* entrapment of MNPs, even though a higher amount of MNPs per amount of HA-derivative was used in the *in situ* method. Taking into account the initial amount of MNPs

used for encapsulation, we found encapsulation efficiency (EE) of 110 % (EE = amount of encapsulated MNPs /amount of initial MNPs x 100%) in the case of core-shell nanobeads, indicating total encapsulation of the used MNPs. We assume that the overrated value of EE is due to the fact that not all polymer chains initially added to the solution were deposited on the clusters. This is coherent with our observation of the solution after attraction of nanobeads towards the bulk magnet (Fig. 2B), where the supernatant stayed slightly cloudy, most probably due to the presence of free polymer which was not implicated in coating. By contrast, incorporation of MNPs by an increase of temperature of thermoresponsive HA resulted in an EE equal to 18%. This indicates that only a small amount of MNPs present initially in solution was used in nanogel formation. Indeed, we observed the formation of hydrophobic MNPs precipitates which accumulated on the vial walls, and only well dispersed nanogels were collected for further analysis.

We could conclude that the formation of MNP nanoclusters followed by deposition of HA-*g*-poly(DEGMA-*co*-BMA) was more efficient to increase the concentration of MNPs in the nanobeads, which in turn increased the magnetic moment and responsiveness to the bulk magnet.

Figure 6A shows ZFC-FC curves for core-shell nanobeads. ZFC magnetization reaches a maximum at 50 K. The increase of the blocking temperature  $T_B$ , when compared to measurements made on a collection of dispersed MNPs presented in Fig. 1B, is attributed to interparticle dipolar interactions resulting from MNP aggregation during cluster formation. Indeed an increase of blocking temperature was previously reported for  $\gamma$ -Fe<sub>2</sub>O<sub>3</sub> NPs concentrated in liposomes.<sup>46</sup> A room temperature  $M(H)$  measurement confirmed that the MNPs preserved their superparamagnetic behavior after clustering and HA-*g*-poly(DEGMA-*co*-BMA) coating since no hysteresis is observed (Fig. 6B). Accordingly, the HA-coated nanobeads could be attracted to the bulk magnet and then easily re-dispersed in its absence.

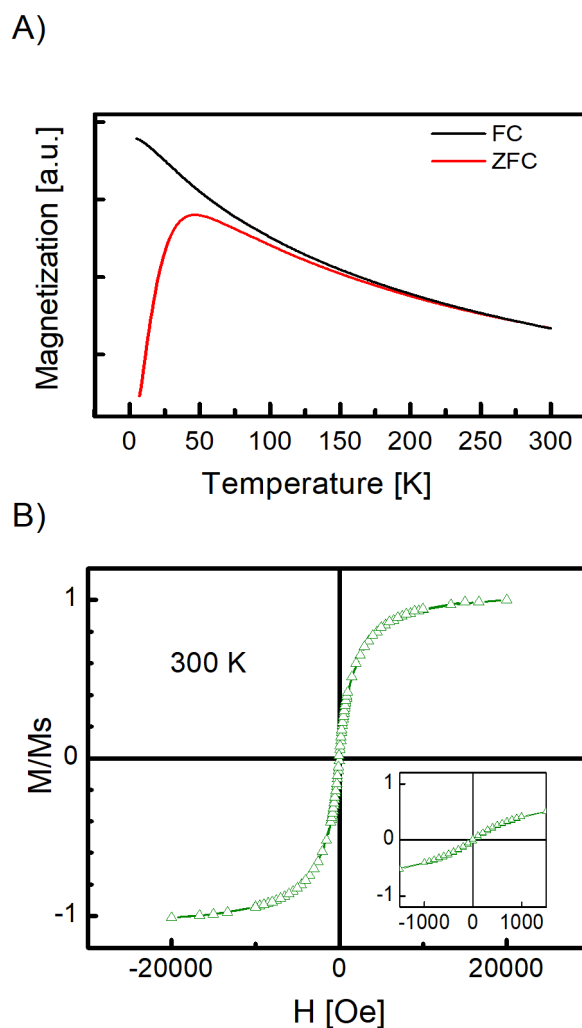


**Figure 6.** A) Temperature dependence of magnetization of HA-g-poly(DEGMA-co-BMA) coated magnetic nanoclusters under ZFC-FC conditions, measured at 100 Oe. B) M/Ms vs H loop of HA-g-poly(DEGMA-co-BMA) coated magnetic nanoclusters at 300 K.

To demonstrate the possibility to magnetically manipulate the nanobeads, we used thermomagnetically micropatterned hard magnetic films characterized by a high remanence (1.2 T) and very high magnetic field gradients ( $<10^6$  T m<sup>-1</sup>), to trap the nanobeads in a controlled fashion. The magnetic nanobeads were first loaded with the di-styrylbenzene derivative (DSB). DSB is a hydrophobic fluorescent dye used as a drug model, as described earlier.<sup>32</sup> The fluorescent dye was mixed with MNPs in THF before cluster formation, sonication in THF/ACN and coating by HA-copolymer chains. The unloaded dye could be

easily removed using the attraction of the magnetic nanobeads to the bulk magnet followed by removal of the supernatant. Figure 7A presents a fluorescence microscopy image of DSB-loaded nanobeads homogeneously dispersed in water. The stability of DSB-loaded magnetic nanobeads was confirmed by DLS analysis (Fig. 4).

To observe the response of nanobeads to the magnetic field pattern produced by micro-magnet arrays, a suspension of fluorescent magnetic nanobeads was dropped onto a glass coverslip and flattened with the thermomagnetically patterned films. The particles dispersed in the solution moved towards the regions of highest magnetic field gradient, which are located at the interfaces between neighboring magnetic zones of opposite magnetization.

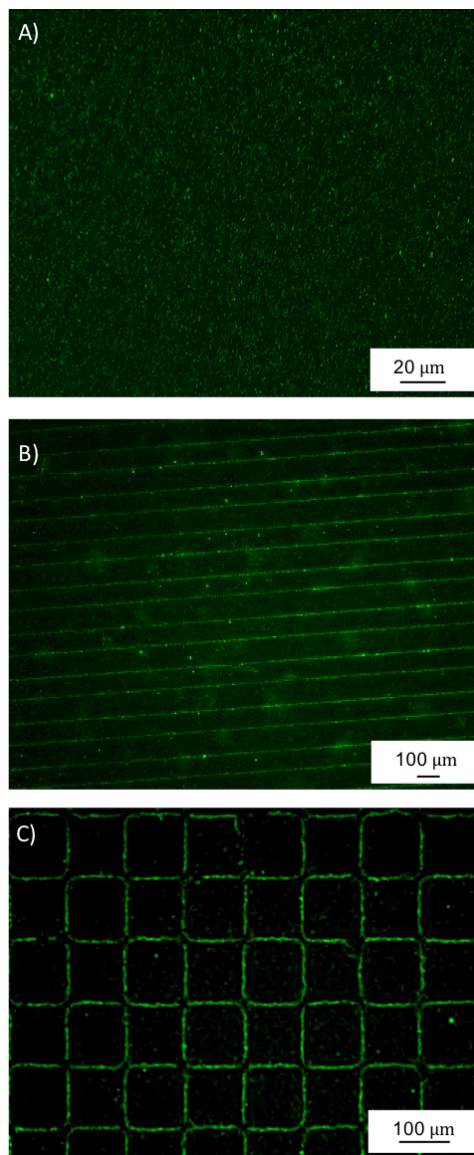


**Figure 7.** Fluorescence microscopy images of DSB-loaded magnetic nanobeads suspended in water (A), and trapped by micro-magnet arrays after 1 min (B,C).

Figure 7B,C presents the images after 1 min of interaction with magnetic arrays with line and square patterns. Nanobeads initially dispersed in the solution (Fig. 7A) are positioned on the top of the micromagnets, creating patterns that reflect the geometry of the underlying magnetic structure. In the case of magnetic stripes, fluorescent lines were observed (Fig. 7B) while in the case of magnetic chessboards, the particles formed fluorescent chessboard patterns (Fig. 7C). After just 1 min, the fluorescence intensity of the magnetic pattern is

essentially stable, indicating that practically all magnetic nanobeads have been trapped. This is in agreement with our previous report on the highly efficient capture of magnetic nanoparticles by these high field gradient micro-magnet arrays.<sup>47</sup> The trapping of some nanobeads away from the interfaces between micro-magnets reflects local inhomogeneities in the stray field pattern produced by thermomagnetically patterned films.<sup>48</sup> The controlled trapping of fluorescent nanobeads using micro-magnet arrays allows for a simple optical verification of the magnetic nature of the nanobeads. The high concentration of superparamagnetic iron oxide nanoparticles in the core of the nanobeads leads to a rapid response to magnetic fields.

#### **4. Conclusions**

We have described the synthesis of HA-based nanobeads loaded with a high content of MNPs. The MNP nanoclusters were first formed and then later coated with HA-g-poly(DEGMA-*co*-BMA). The HA derivative perfectly stabilized the magnetic nanoclusters in aqueous solution. Additionally, we showed the possibility of cluster formation in the presence of a model fluorescent drug, which demonstrates the possibility of simultaneous introduction of two functions: magnetic properties and drug encapsulation. Thanks to the relatively high concentration of MNPs within the bead core, a bulk magnet could be used for sample purification and nanobead separation. Micro-magnet arrays characterized by high-field gradients were shown to trap the nanobeads in a very short time. The study of magnetic attraction and controlled positioning could be extended to the guiding of drug-loaded magnetic nanobeads towards specific organs within the body.

#### **Conflicts of interest**

The authors declare no conflicts of interest.

## Acknowledgements

M. Rippe gratefully acknowledges the Ministère de l'Enseignement Supérieur, de la Recherche et de l'Innovation (MESRI) for her doctoral training grant. This work was partially supported by LabEx Arcane (Investissements d'Avenir, grant agreement #ANR-11-LABX-0003-01). The FEG-SEM images were recorded at the CMTC characterization platform of Grenoble INP supported by LabEx CEMAM (Investissements d'Avenir, grant agreement #ANR-10-LABX-44-01). We thank Francine Roussel-Dherbey (CMTC) for the FEG-SEM observations, Sonia Ortega (CERMAV) for TGA measurements, and the NanoBio-ICMG platform (FR 2607, Grenoble) for granting access to the TEM facility.

## Appendix A. Supplementary material

Supplementary data to this article can be found online at <http://.....>

## References

- (1) Wu, W.; Wu, Z.; Yu, T.; Jiang, C.; Kim, W.-S. Recent Progress on Magnetic Iron Oxide Nanoparticles: Synthesis, Surface Functional Strategies and Biomedical Applications. *Sci. Technol. Adv. Mater.* **2015**, *16* (2), 023501. <https://doi.org/10.1088/1468-6996/16/2/023501>.
- (2) Di Corato, R.; Béalle, G.; Kolosnjaj-Tabi, J.; Espinosa, A.; Clément, O.; Silva, A. K. A.; Ménager, C.; Wilhelm, C. Combining Magnetic Hyperthermia and Photodynamic Therapy for Tumor Ablation with Photoresponsive Magnetic Liposomes. *ACS Nano* **2015**, *9* (3), 2904–2916. <https://doi.org/10.1021/nn506949t>.
- (3) Glover, A. L.; Bennett, J. B.; Pritchett, J. S.; Nikles, S. M.; Nikles, D. E.; Nikles, J. A.; Brazel, C. S. Magnetic Heating of Iron Oxide Nanoparticles and Magnetic Micelles for Cancer Therapy. *IEEE Trans. Magn.* **2013**, *49* (1), 231–235. <https://doi.org/10.1109/TMAG.2012.2222359>.
- (4) Oliveira, H.; Pérez-Andrés, E.; Thevenot, J.; Sandre, O.; Berra, E.; Lecommandoux, S. Magnetic Field Triggered Drug Release from Polymersomes for Cancer Therapeutics. *J. Controlled Release* **2013**, *169* (3), 165–170. <https://doi.org/10.1016/j.jconrel.2013.01.013>.
- (5) Cazares-Cortes, E.; Espinosa, A.; Guigner, J.-M.; Michel, A.; Griffete, N.; Wilhelm, C.; Ménager, C. Doxorubicin Intracellular Remote Release from Biocompatible Oligo(Ethylene Glycol) Methyl Ether Methacrylate-Based Magnetic Nanogels

- Triggered by Magnetic Hyperthermia. *ACS Appl. Mater. Interfaces* **2017**, *9* (31), 25775–25788. <https://doi.org/10.1021/acsami.7b06553>.
- (6) Odrobińska, J.; Gumieniczek-Chłopek, E.; Szuwarzyński, M.; Radziszewska, A.; Fiejdasz, S.; Strączek, T.; Kapusta, C.; Zapotoczny, S. Magnetically Navigated Core–Shell Polymer Capsules as Nanoreactors Loadable at the Oil/Water Interface. *ACS Appl. Mater. Interfaces* **2019**, *11* (11), 10905–10913. <https://doi.org/10.1021/acsami.8b22690>.
  - (7) Pavlov, A. M.; Geest, B. G. D.; Louage, B.; Lybaert, L.; Koker, S. D.; Koudelka, Z.; Sapelkin, A.; Sukhorukov, G. B. Magnetically Engineered Microcapsules as Intracellular Anchors for Remote Control Over Cellular Mobility. *Adv. Mater.* **2013**, *25* (48), 6945–6950. <https://doi.org/10.1002/adma.201303287>.
  - (8) Zhu, L.; Ma, J.; Jia, N.; Zhao, Y.; Shen, H. Chitosan-Coated Magnetic Nanoparticles as Carriers of 5-Fluorouracil: Preparation, Characterization and Cytotoxicity Studies. *Colloids Surf. B Biointerfaces* **2009**, *68* (1), 1–6. <https://doi.org/10.1016/j.colsurfb.2008.07.020>.
  - (9) You, D. G.; Saravanakumar, G.; Son, S.; Han, H. S.; Heo, R.; Kim, K.; Kwon, I. C.; Lee, J. Y.; Park, J. H. Dextran Sulfate-Coated Superparamagnetic Iron Oxide Nanoparticles as a Contrast Agent for Atherosclerosis Imaging. *Carbohydr. Polym.* **2014**, *101*, 1225–1233. <https://doi.org/10.1016/j.carbpol.2013.10.068>.
  - (10) Hong, R. Y.; Li, J. H.; Qu, J. M.; Chen, L. L.; Li, H. Z. Preparation and Characterization of Magnetite/Dextran Nanocomposite Used as a Precursor of Magnetic Fluid. *Chem. Eng. J.* **2009**, *150* (2), 572–580. <https://doi.org/10.1016/j.cej.2009.03.034>.
  - (11) Ma, H.; Qi, X.; Maitani, Y.; Nagai, T. Preparation and Characterization of Superparamagnetic Iron Oxide Nanoparticles Stabilized by Alginate. *Int. J. Pharm.* **2007**, *333* (1), 177–186. <https://doi.org/10.1016/j.ijpharm.2006.10.006>.
  - (12) Lee, J.; Jung, M. J.; Hwang, Y. H.; Lee, Y. J.; Lee, S.; Lee, D. Y.; Shin, H. Heparin-Coated Superparamagnetic Iron Oxide for in Vivo MR Imaging of Human MSCs. *Biomaterials* **2012**, *33* (19), 4861–4871. <https://doi.org/10.1016/j.biomaterials.2012.03.035>.
  - (13) Cheng, Z.; Liu, S.; Gao, H.; Tremel, W.; Ding, N.; Liu, R.; Beines, P. W.; Knoll, W. A Facile Approach for Transferring Hydrophobic Magnetic Nanoparticles into Water-Soluble Particles. *Macromol. Chem. Phys.* **2008**, *209* (11), 1145–1151. <https://doi.org/10.1002/macp.200800085>.
  - (14) Jiang, L.; Zhou, Q.; Mu, K.; Xie, H.; Zhu, Y.; Zhu, W.; Zhao, Y.; Xu, H.; Yang, X. PH/Temperature Sensitive Magnetic Nanogels Conjugated with Cy5.5-Labeled Lactoferrin for MR and Fluorescence Imaging of Glioma in Rats. *Biomaterials* **2013**, *34* (30), 7418–7428. <https://doi.org/10.1016/j.biomaterials.2013.05.078>.
  - (15) Deka, S. R.; Quarta, A.; Corato, R. D.; Riedinger, A.; Cingolani, R.; Pellegrino, T. Magnetic Nanobeads Decorated by Thermo-Responsive PNIPAM Shell as Medical Platforms for the Efficient Delivery of Doxorubicin to Tumour Cells. *Nanoscale* **2011**, *3* (2), 619–629. <https://doi.org/10.1039/C0NR00570C>.
  - (16) Tripodo, G.; Trapani, A.; Torre, M. L.; Giammona, G.; Trapani, G.; Mandracchia, D. Hyaluronic Acid and Its Derivatives in Drug Delivery and Imaging: Recent Advances and Challenges. *Eur. J. Pharm. Biopharm.* **2015**, *97*, 400–416. <https://doi.org/10.1016/j.ejpb.2015.03.032>.
  - (17) Auzenne, E.; Ghosh, S. C.; Khodadadian, M.; Rivera, B.; Farquhar, D.; Price, R. E.; Ravoori, M.; Kundra, V.; Freedman, R. S.; Klostergaard, J. Hyaluronic Acid-Paclitaxel: Antitumor Efficacy against CD44(+) Human Ovarian Carcinoma Xenografts. *Neoplasia* **2007**, *9* (6), 479–486. <https://doi.org/10.1593/neo.07229>.

- (18) Draffin, J. E.; McFarlane, S.; Hill, A.; Johnston, P. G.; Waugh, D. J. J. CD44 Potentiates the Adherence of Metastatic Prostate and Breast Cancer Cells to Bone Marrow Endothelial Cells. *Cancer Res.* **2004**, *64* (16), 5702–5711. <https://doi.org/10.1158/0008-5472.CAN-04-0389>.
- (19) Babic, M.; Horak, D.; Jendelova, P.; Herynek, V.; Proks, V.; Vanecek, V.; Lesny, P.; Sykova, E. The Use of Dopamine-Hyaluronate Associate-Coated Maghemite Nanoparticles to Label Cells. *Int. J. Nanomedicine* **2012**, *7*, 1461–1474. <https://doi.org/10.2147/IJN.S28658>.
- (20) Lee, Y.; Lee, H.; Kim, Y. B.; Kim, J.; Hyeon, T.; Park, H.; Messersmith, P. B.; Park, T. G. Bioinspired Surface Immobilization of Hyaluronic Acid on Monodisperse Magnetite Nanocrystals for Targeted Cancer Imaging. *Adv. Mater.* **2008**, *20* (21), 4154–4157. <https://doi.org/10.1002/adma.200800756>.
- (21) Thomas, R. G.; Moon, M. J.; Lee, H.; Sasikala, A. R. K.; Kim, C. S.; Park, I.-K.; Jeong, Y. Y. Hyaluronic Acid Conjugated Superparamagnetic Iron Oxide Nanoparticle for Cancer Diagnosis and Hyperthermia Therapy. *Carbohydr. Polym.* **2015**, *131*, 439–446. <https://doi.org/10.1016/j.carbpol.2015.06.010>.
- (22) Manju, S.; Sreenivasan, K. Enhanced Drug Loading on Magnetic Nanoparticles by Layer-by-Layer Assembly Using Drug Conjugates: Blood Compatibility Evaluation and Targeted Drug Delivery in Cancer Cells. *Langmuir* **2011**, *27* (23), 14489–14496. <https://doi.org/10.1021/la202470k>.
- (23) El-Dakdouki, M. H.; Zhu, D. C.; El-Boubbou, K.; Kamat, M.; Chen, J.; Li, W.; Huang, X. Development of Multifunctional Hyaluronan-Coated Nanoparticles for Imaging and Drug Delivery to Cancer Cells. *Biomacromolecules* **2012**, *13* (4), 1144–1151. <https://doi.org/10.1021/bm300046h>.
- (24) Jia, Y.; Fan, M.; Chen, H.; Miao, Y.; Xing, L.; Jiang, B.; Cheng, Q.; Liu, D.; Bao, W.; Qian, B.; et al. Magnetic Hyaluronic Acid Nanospheres via Aqueous Diels–Alder Chemistry to Deliver Dexamethasone for Adipose Tissue Engineering. *J. Colloid Interface Sci.* **2015**, *458*, 293–299. <https://doi.org/10.1016/j.jcis.2015.07.062>.
- (25) Maity, D.; Ding, J.; Xue, J.-M. Synthesis of Magnetite Nanoparticles by Thermal Decomposition: Time, Temperature, Surfactant and Solvent Effects. *Funct. Mater. Lett.* **2008**, *01* (03), 189–193. <https://doi.org/10.1142/S1793604708000381>.
- (26) Mosafer, J.; Abnous, K.; Tafaghodi, M.; Jafarzadeh, H.; Ramezani, M. Preparation and Characterization of Uniform-Sized PLGA Nanospheres Encapsulated with Oleic Acid-Coated Magnetic-Fe<sub>3</sub>O<sub>4</sub> Nanoparticles for Simultaneous Diagnostic and Therapeutic Applications. *Colloids Surf. Physicochem. Eng. Asp.* **2017**, *514*, 146–154. <https://doi.org/10.1016/j.colsurfa.2016.11.056>.
- (27) Šmejkalová, D.; Nešporová, K.; Huerta-Angeles, G.; Syrovátka, J.; Jiráček, D.; Gálisová, A.; Velebný, V. Selective In Vitro Anticancer Effect of Superparamagnetic Iron Oxide Nanoparticles Loaded in Hyaluronan Polymeric Micelles. *Biomacromolecules* **2014**, *15* (11), 4012–4020. <https://doi.org/10.1021/bm501065q>.
- (28) Lim, E.-K.; Kim, H.-O.; Jang, E.; Park, J.; Lee, K.; Suh, J.-S.; Huh, Y.-M.; Haam, S. Hyaluronan-Modified Magnetic Nanoclusters for Detection of CD44-Overexpressing Breast Cancer by MR Imaging. *Biomaterials* **2011**, *32* (31), 7941–7950. <https://doi.org/10.1016/j.biomaterials.2011.06.077>.
- (29) Stern, R.; Kogan, G.; Jedrzejewski, M. J.; Šoltés, L. The Many Ways to Cleave Hyaluronan. *Biotechnol. Adv.* **2007**, *25* (6), 537–557. <https://doi.org/10.1016/j.biotechadv.2007.07.001>.
- (30) Talelli, M.; Rijcken, C. J. F.; Lammers, T.; Seevinck, P. R.; Storm, G.; van Nostrum, C. F.; Hennink, W. E. Superparamagnetic Iron Oxide Nanoparticles Encapsulated in Biodegradable Thermosensitive Polymeric Micelles: Toward a Targeted Nanomedicine

- Suitable for Image-Guided Drug Delivery. *Langmuir* **2009**, *25* (4), 2060–2067. <https://doi.org/10.1021/la8036499>.
- (31) Di Corato, R.; Piacenza, P.; Musarò, M.; Buonsanti, R.; Cozzoli, P. D.; Zambianchi, M.; Barbarella, G.; Cingolani, R.; Manna, L.; Pellegrino, T. Magnetic–Fluorescent Colloidal Nanobeads: Preparation and Exploitation in Cell Separation Experiments. *Macromol. Biosci.* **2009**, *9* (10), 952–958. <https://doi.org/10.1002/mabi.200900154>.
- (32) Fernandes Stefanello, T.; Szarpak-Jankowska, A.; Appaix, F.; Louage, B.; Hamard, L.; De Geest, B. G.; van der Sanden, B.; Nakamura, C. V.; Auzély-Velty, R. Thermoresponsive Hyaluronic Acid Nanogels as Hydrophobic Drug Carrier to Macrophages. *Acta Biomater.* **2014**, *10* (11), 4750–4758. <https://doi.org/10.1016/j.actbio.2014.07.033>.
- (33) Garcia, F. P.; Rippe, M.; Companhoni, M. V. P.; Stefanello, T. F.; Louage, B.; Herck, S. V.; Sancey, L.; Coll, J.-L.; Geest, B. G. D.; Nakamura, C. V.; et al. A Versatile Method for the Selective Core-Crosslinking of Hyaluronic Acid Nanogels via Ketone-Hydrazide Chemistry: From Chemical Characterization to in Vivo Biodistribution. *Biomater. Sci.* **2018**, *6* (7), 1754–1763. <https://doi.org/10.1039/C8BM00396C>.
- (34) Stefanello, T. F.; Couturaud, B.; Szarpak-Jankowska, A.; Fournier, D.; Louage, B.; Garcia, F. P.; Nakamura, C. V.; Geest, B. G. D.; Woisel, P.; Sanden, B. van der; et al. Coumarin-Containing Thermoresponsive Hyaluronic Acid-Based Nanogels as Delivery Systems for Anticancer Chemotherapy. *Nanoscale* **2017**, *9* (33), 12150–12162. <https://doi.org/10.1039/C7NR03964F>.
- (35) Rippe, M.; Stefanello, T. F.; Kaplum, V.; Britta, E. A.; Garcia, F. P.; Poirot, R.; Companhoni, M. V. P.; Nakamura, C. V.; Szarpak-Jankowska, A.; Auzély-Velty, R. Heparosan as a Potential Alternative to Hyaluronic Acid for the Design of Biopolymer-Based Nanovectors for Anticancer Therapy. *Biomater. Sci.* **2019**, *7* (7), 2850–2860. <https://doi.org/10.1039/C9BM00443B>.
- (36) Bitter, T.; Muir, H. M. A Modified Uronic Acid Carbazole Reaction. *Anal. Biochem.* **1962**, *4* (4), 330–334. [https://doi.org/10.1016/0003-2697\(62\)90095-7](https://doi.org/10.1016/0003-2697(62)90095-7).
- (37) Moya, C.; Batlle, X.; Labarta, A. The Effect of Oleic Acid on the Synthesis of Fe<sub>3</sub>O<sub>4</sub> Nanoparticles over a Wide Size Range. *Phys. Chem. Chem. Phys.* **2015**, *17* (41), 27373–27379. <https://doi.org/10.1039/C5CP03395K>.
- (38) Palma, S. I. C. J.; Marciello, M.; Carvalho, A.; Veintemillas-Verdaguer, S.; Morales, M. del P.; Roque, A. C. A. Effects of Phase Transfer Ligands on Monodisperse Iron Oxide Magnetic Nanoparticles. *J. Colloid Interface Sci.* **2015**, *437*, 147–155. <https://doi.org/10.1016/j.jcis.2014.09.019>.
- (39) Sun, S.; Zeng, H.; Robinson, D. B.; Raoux, S.; Rice, P. M.; Wang, S. X.; Li, G. Monodisperse MFe<sub>2</sub>O<sub>4</sub> (M = Fe, Co, Mn) Nanoparticles. *J. Am. Chem. Soc.* **2004**, *126* (1), 273–279. <https://doi.org/10.1021/ja0380852>.
- (40) Dumas-Bouchiat, F.; Zanini, L. F.; Kustov, M.; Dempsey, N. M.; Grechishkin, R.; Hasselbach, K.; Orlianges, J. C.; Champeaux, C.; Catherinot, A.; Givord, D. Thermomagnetically Patterned Micromagnets. *Appl. Phys. Lett.* **2010**, *96* (10), 102511. <https://doi.org/10.1063/1.3341190>.
- (41) Kustov, M.; Laczkowski, P.; Hykel, D.; Hasselbach, K.; Dumas-Bouchiat, F.; O'Brien, D.; Kauffmann, P.; Grechishkin, R.; Givord, D.; Reyne, G.; et al. Magnetic Characterization of Micropatterned Nd–Fe–B Hard Magnetic Films Using Scanning Hall Probe Microscopy. *J. Appl. Phys.* **2010**, *108* (6), 063914. <https://doi.org/10.1063/1.3486513>.
- (42) Yu, W. W.; Falkner, J. C.; Yavuz, C. T.; Colvin, V. L. Synthesis of Monodisperse Iron Oxide Nanocrystals by Thermal Decomposition of Iron Carboxylate Salts. *Chem. Commun.* **2004**, No. 20, 2306–2307. <https://doi.org/10.1039/B409601K>.

- (43) Bronstein, L. M.; Huang, X.; Retrum, J.; Schmucker, A.; Pink, M.; Stein, B. D.; Dragnea, B. Influence of Iron Oleate Complex Structure on Iron Oxide Nanoparticle Formation. *Chem. Mater.* **2007**, *19* (15), 3624–3632. <https://doi.org/10.1021/cm062948j>.
- (44) Zhang, L.; He, R.; Gu, H.-C. Oleic Acid Coating on the Monodisperse Magnetite Nanoparticles. *Appl. Surf. Sci.* **2006**, *253* (5), 2611–2617. <https://doi.org/10.1016/j.apsusc.2006.05.023>.
- (45) Sheu, C.; T. Shalumon, K.; Chen, C.-H.; Kuo, C.-Y.; Teng Fong, Y.; Chen, J.-P. Dual Crosslinked Hyaluronic Acid Nanofibrous Membranes for Prolonged Prevention of Post-Surgical Peritoneal Adhesion. *J. Mater. Chem. B* **2016**, *4* (41), 6680–6693. <https://doi.org/10.1039/C6TB01376G>.
- (46) Di Corato, R.; Espinosa, A.; Lartigue, L.; Tharaud, M.; Chat, S.; Pellegrino, T.; Ménager, C.; Gazeau, F.; Wilhelm, C. Magnetic Hyperthermia Efficiency in the Cellular Environment for Different Nanoparticle Designs. *Biomaterials* **2014**, *35* (24), 6400–6411. <https://doi.org/10.1016/j.biomaterials.2014.04.036>.
- (47) Fratzl, M.; Delshadi, S.; Devillers, T.; Bruckert, F.; Cugat, O.; Dempsey, N. M.; Blaire, G. Magnetophoretic Induced Convective Capture of Highly Diffusive Superparamagnetic Nanoparticles. *Soft Matter* **2018**, *14* (14), 2671–2681. <https://doi.org/10.1039/C7SM02324C>.
- (48) Ponomareva, S.; Dias, A.; Royer, B.; Marelli, H.; Motte, J. F.; Givord, D.; Dumas-Bouchiat, F.; Dempsey, N. M.; Marchi, F. A Quantitative Study of Magnetic Interactions between a Micro-Magnet Array and Individual Magnetic Micro-Particles by Scanning Particle Force Microscopy. *J. Micromechanics Microengineering* **2019**, *29* (1), 015010. <https://doi.org/10.1088/1361-6439/aaefd5>.